Lean partially premixed turbulent flame equivalence ratio measurements using laser-induced breakdown spectroscopy

Badawy, T, Hamza, M, Mansour, MS, Abdel-Hafez, AHH, Imam, H, Abdel-Raheem, MA, Wang, C & Lattimore, T

Original citation & hyperlink:

Badawy, T, Hamza, M, Mansour, MS, Abdel-Hafez, AHH, Imam, H, Abdel-Raheem, MA, Wang, C & Lattimore, T 2019, 'Lean partially premixed turbulent flame equivalence ratio measurements using laser-induced breakdown spectroscopy' Fuel, vol. 237, pp. 320-334.

https://dx.doi.org/10.1016/j.fuel.2018.10.015

DOI 10.1016/j.fuel.2018.10.015

ISSN 0016-2361

Publisher: Elsevier

Lean partially premixed turbulent flame equivalence ratio measurements using Laser-induced breakdown spectroscopy

Tawfik Badawy [a*], Mahmoud Hamza [a], Mohy S. Mansour [a, b], Abdel-Hafez H. Abdel-Hafez [a], Hisham Imam [c], Mohamed A. Abdel-Raheem [d], Chongming Wang [e], Thomas Lattimore [f]

[a] Mechanical Power Engineering Department, Cairo University, Egypt.
[b] Mechanical Engineering Department, The American University in Cairo, Egypt
[c] National Institute of Laser Enhanced Sciences, Cairo University, Giza, Egypt
[d] School of Engineering and Sustainable Development, De Montfort University, Leicester, UK
[e] School of Mechanical, Aerospace and Automotive Engineering, Coventry University, Coventry, UK
[f] Department of Engineering, German University of Technology, Oman.

*Corresponding author at: Cairo University, Egypt. E-mail address: tsb308@outlook.com (T. Badawy).

Abstract

The creation of a more stable flame along with the extension of flammability limits under lean mixture combustion was the main motivation to develop a new burner design, which has been investigated in this research. The current burner configuration was utilized to create a wide range of higher turbulent intensities and to produce different degrees of mixture inhomogeneity, which acted to promote minimum pollution, highest performance and higher flame stability. The burner stability assessment was investigated using two types of fuel: natural gas (NG) and liquefied petroleum gas (LPG). They were tested under different degrees of partial premixing, and two turbulence generator disks for lean mixture at an equivalence ratio of φ = 0.8 were used. Following this, the Laser Induced Breakdown Spectroscopy (LIBS) technique was utilized to characterize and quantify the impact of changing the disk slit diameter on the distributions profiles of equivalence ratio or mixture fraction for a NG/air partially premixed flame. A series of homogeneous NG/air mixtures with different equivalence ratios were used to obtain the correlations between the measured emission lines of LIBS spectra and the global flame equivalence ratio. Consequently, the emission spectral lines ratios of H/N, H/O and C/N+O were utilized to predict the equivalence ratio distributions. The results demonstrated that for all of the mixing lengths, NG/air mixture with larger disk generator diameter yielded the maximum burner stability, whilst the LPG/air mixture with a larger disk generator diameter resulted in the minimum burner stability. Furthermore, the flame associated with the larger disk slit diameter had a uniform local equivalence ratio distribution and lower RMS fluctuation profiles of equivalence ratio in comparison to the lower disk slit diameter.

Keywords: Stability; laser breakdown; partially premixed; Turbulence; LIBS; Mixture fraction

Highlights:

- Fuel type and partially premixed level effects on burner stability
- Flame stability behaviour of different turbulence generator disks were investigated
- Impact of changing the disk slit diameter on equivalence ratio distributions was examined

Nomenclature

LIBS	laser induced breakdown spectroscopy	Y_{fi}	Mass fractions of the fuel elements
d_s	Turbulence generator diameter	L_k	Kolmogorov scale
ξ	Mixture fraction	HI	Hydrogen intensity
NG	Natural gas	λ	Laser wavelength
PPFs	Partially Premixed Flames	V_j	Jet velocity
ICCD	Intensified Charge-coupled device	τ_{mix}	Mixing time
L	Mixing length, mm	φ	Equivalence ratio
b	Slit thickness	d_C	Cone diameter
LTE	Local Thermal Equilibrium	X	Axial distance above the burner tip
C_3H_8	Propane	C_4H_{10}	Butane
Rms	Root mean square	δ	Convection-diffusion laminar flame thickness
PI	Princeton Instruments		
NI	Nitrogen intensity	OI	Oxygen intensity
CI	Carbon intensity	θ	Cone half angle
D	Inner diameter of the outer tube, mm	d	Inner diameter of the inner tube, mm
Do	Outer diameter of the outer tube, mm	do	Outer diameter of the inner tube, mm
r	Radial distance, mm	X	Axial distance, mm
R	Inner radius of the outer tube, mm		

Introduction

The mixture stratification process and the generation of higher turbulence levels are the two main established techniques to extend the lean combustion limit [1]. Therefore, the new combustion system design, directed towards partially premixing combustion, is a promising technology, which offers the potential to meet ever stringent emission regulations, as well as improving the system efficiency [2]. The performance of the combustion processes is mainly linked to the local equivalence ratio distributions near the ignition event, and based on these distributions, the combustion characteristics and the level of emissions such as CO, NOx, etc. will be strongly affected [3, 4]. This influence is mainly linked to the change of both the local properties of the reaction zone and the global behaviour of the combustion system associated with the flame propagation within spatial variations of the equivalence ratio [5]. Therefore, quantifications of this ratio are essential to sustain the higher stability of the combustion process and to minimize the soot emissions [6].

Richardson et al. [7] demonstrated that the laminar flame propagation speed was affected by the equivalence ratio gradients, due to the gradients effects on the molecular transport of hot products and radical species into the reaction zone. Furthermore, Dold [8] concluded that as the mixture fraction or equivalence ratio gradient increased, the flame propagation speed was reduced. This was attributed to the lower conduction heat transfer associated with the increased flame front curvature, which consequently reduced the preheating process of the unburned mixture. Likewise, Richardson and Chen [4] investigated turbulent flame propagation under the impacts of equivalence ratio-stratification for methane air flame using DNS analysis. They concluded that the stratification process influences significantly on the flame surface area due to the variation caused by equivalence ratio gradient orientation on the flame surface averaged consumption speed with surface averaged equivalence ratio.

In order to measure and obtain comprehensive information regarding global and local equivalence ratios distributions in turbulent flames, laser induced break down spectroscopy (LIBS) was used in this research. The principle of laser induced breakdown spectroscopy depends mainly on the interaction of a very short-duration focused pulsed laser beam onto the surface of the substance to be analysed, causing the breakdown of the sample's chemical bonds, followed by the formation of plasma, which is composed of ionized matter [9, 10]. During the subsequent relaxation of the constituent excited species, the spectral emission occurred, and it was collected and spectrographically analysed using an Intensified CCD (ICCD) detector attached to a spectrograph detector [11]. The elemental composition of any material can be identified based on their fingerprint spectral lines, and consequently, the concentration of such elements will be quantified from the spectral line intensities. The main advantages of the LIBS technique lies in its ability to rapidly analyse samples remotely and in situ, with minimal sample preparation [12, 13]. Furthermore, LIBS has the potential of simultaneous multi-elemental analysis with minimum equipment [14]. The aforementioned advantages make the LIBS technique to an attractive tool for the majority of applications including liquids [15, 16], solids [17, 18] and quantitiative analysis of gases and gas mixtures, which are all essential tasks in the field of security, environmental and chemical enalysis [19, 20].

Over the past few years, the LIBS technique has been applied extensively to the field of combustion diagnostics [21, 22] for equivalence ratio measurements which can be obtained based on the atomic species concentrations in flames. Kotzagianni et al. [23] established a new calibration scheme for equivalence ratio measurements of non-premixed and premixed methane turbulent flames using the LIBS technique. They concluded that for a lower mole fraction of methane in the range 0-0.3, the ratio of Hα (656.3 nm) over O (777.3 nm), (Hα/O), should be utilized for equivalence ratio calculations. Additionally, they found that, for a higher mole fraction of methane in the range 0.3-1, the ratio of C_2 over CN, (C_2/CN), should be used to identify the equivalence ratio. The majority of past LIBS studies were mainly focused on using the ratios of some spectral lines of the atomic origin, such as the carbon line to nitrogen [C (833 nm)/N (744 nm)], the carbon line to oxygen [C (833 nm)/O (777 nm)] [24], or the ratio of the intensity of a carbon line to the sum of the intensities of a nitrogen and an oxygen line, [C (711 nm)]/[N (744 nm) + O (777nm)] [25]. These ratios have been successfully utilized to delineate the relationship between the spectral intensity and the mixture equivalence ratio. The most commonly used ratios were between the hydrogen line to an atomic emission of oxygen line [Hα (656.3 nm)/O (777nm)] or hydrogen line to an atomic emission of nitrogen [Hα (656.3 nm)/N (746.8nm)] [26-28]. Alongside the equivalence ratio measurements, LIBS has been utilized for further analysis of the turbulent flame characteristics, including the measurements of temperature [28], gas density and concentration [29].

The present work discusses the development of a new burner design, which has the ability to operate over lean combustion conditions with higher flame stability, and consequently, it provides lower levels of exhaust emissions. This burner generates different stratification degrees of the mixture by changing the degree of the partially premixed level or by using different turbulent generator disks. Considerable attention has been paid to obtain comprehensive information regarding the impact of changing the disk slit diameter, fuel type and the level of partially premixed on the flame stability maps. The stability map results were examined and utilized to identify the suitable mixture conditions for equivalence ratios distributions using the LIBS technique. Likewise, the ability to conduct quantitative equivalence ratio measurements of partially premixed NG/air mixtures using the LIBS technique was examined. Furthermore, the correlation of values of emission intensity ratio [C/(N+O), H/O and H/N] using LIBS against NG/air mixtures equivalence ratios was established.

2.1. Burner setup details

The new design of the current burner configuration was comprised of a pair of fixed concentric stainless-steel tubes; the inner tube carried the air whilst the outer tube carried the fuel, as shown in Figure 1.

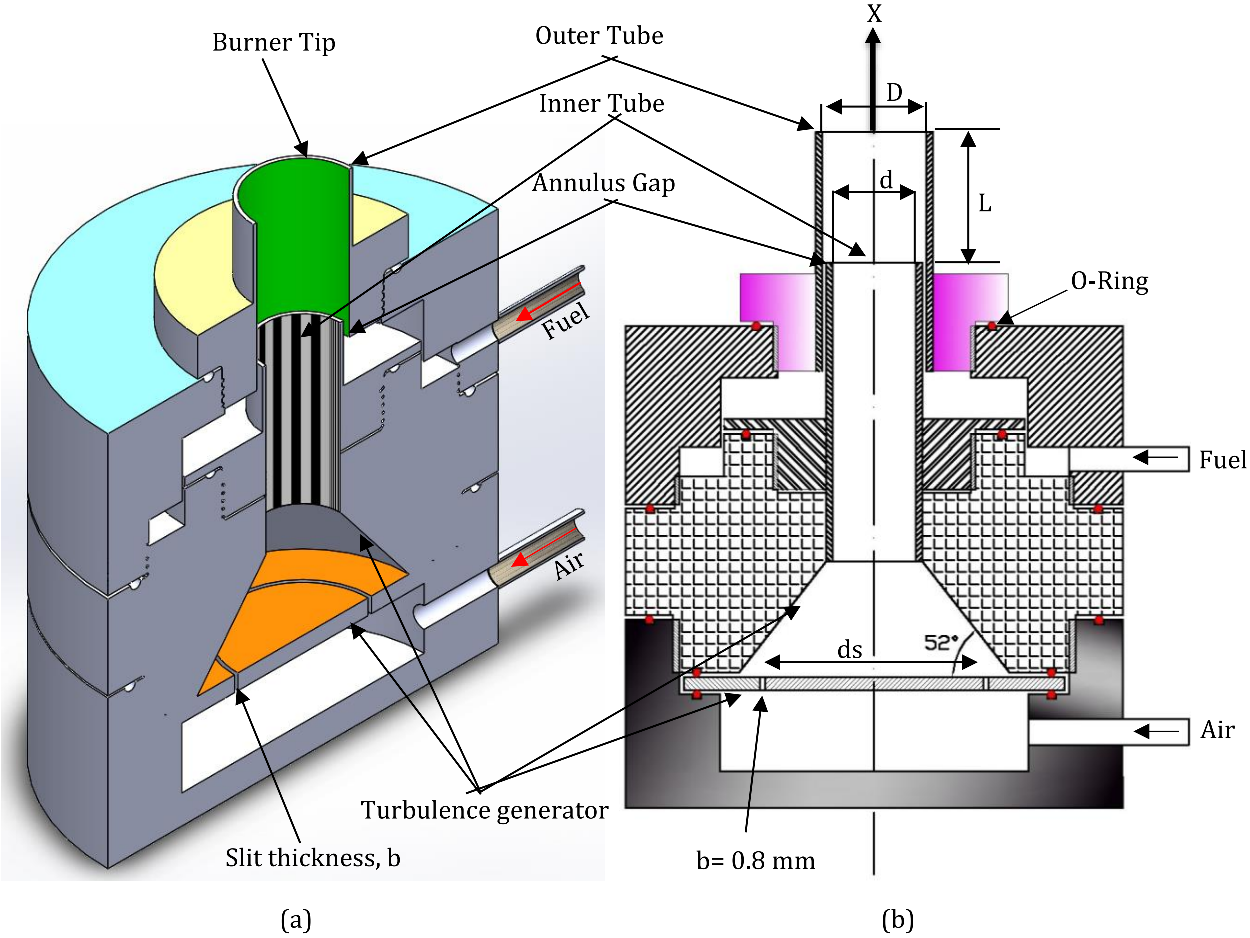

Figure.1. Burner schematic diagram (a) half section 3D sketch, (b) half section 2D sketch

This new burner has the strength to generate higher levels of turbulence intensities as well as the ability to provide different degrees of partial premixing. The inner tube has a wall thickness of 1.5 mm and an inner diameter of d =19 mm, whilst the outer tube has a wall thickness of 1.5 mm and an inner diameter of D = 24 mm. The outlet of the inner tube was located at a distance L below the tip of the outer tube. The mixing process between air and fuel occurred within this distance L, and consequently, by changing this distance, the degree of inhomogeneity was varied. The degree of partial premixing was defined by the ratio L/D and five sets of L/D = 1, 2, 3, 4 and 7 were selected to investigate the burner stability as shown in Figure 2 (a). Both the air and fuel streams were fed into the burner tangentially and directed towards the inner and outer tubes, respectively. The fuel stream passed through the annulus gap between the vertical concentric tubes and then it mixed with the air through the mixing distance, L, as shown in Figure 1. The LPG used during the present study was formed of 50% butane and 50% propane (molar basis). While the NG was formed from of 95% methane (molar basis). The flow rates of both air and fuel streams were controlled precisely using an Alicat MCS-series meter which was calibrated to a certain range of 150 l/min with a high accuracy of ± (0.4% of Reading and + 0.2% of Full Scale). Additionally, it had a 10-millisecond response time. Both the fuel and air streams were introduced to the burner at ambient conditions. The overall mean equivalence ratio was determined based on the fuel and air stream mass flow rates.

2.2. Turbulence generator disks

The turbulence generator used for the current study consisted of a thin disk turbulence generator with a circular slot, in order to boost the turbulence intensity levels, similar to the disk developed by Videto and Santavicca [30]. Beyond this disk, a contracting nozzle was utilized to assist the collapse of the air stream, which passed through the circular slot, into a wide range of turbulent fluctuations and integral length scales, and consequently, this promoted higher levels of turbulence intensities [31]. Recently, several studies have been conducted to develop new turbulence generator designs in order to increase the turbulent flame speed and to achieve improved flame stability [32]. In this paper, two disks with a circular slit diameter of ds= 25 and 45 mm have been selected, as shown in Figure 2 (b). Both the disks were designed with a constant slit thickness (b) of 0.8 mm, whilst the following converging nozzle consisted of a cone angle (2θ) of 76°, 26 mm height (h) and 62 mm base cone diameter (dc). At a partial premixing level of (L/D = 2), a particle image velocimetry (PIV) system was utilized to study the velocity profiles of the developed burner. Accordingly, the flow turbulent intensities were calculated as a ratio between the fluctuation of the jet velocity to the mean jet velocity (V_{rms}/V_j) [33]. They demonstrated that the current burner turbulent intensity could reach up to 36%, depending on the jet velocity, and any increase in the jet velocity or the disk slit diameter will increase the turbulent intensity [33].

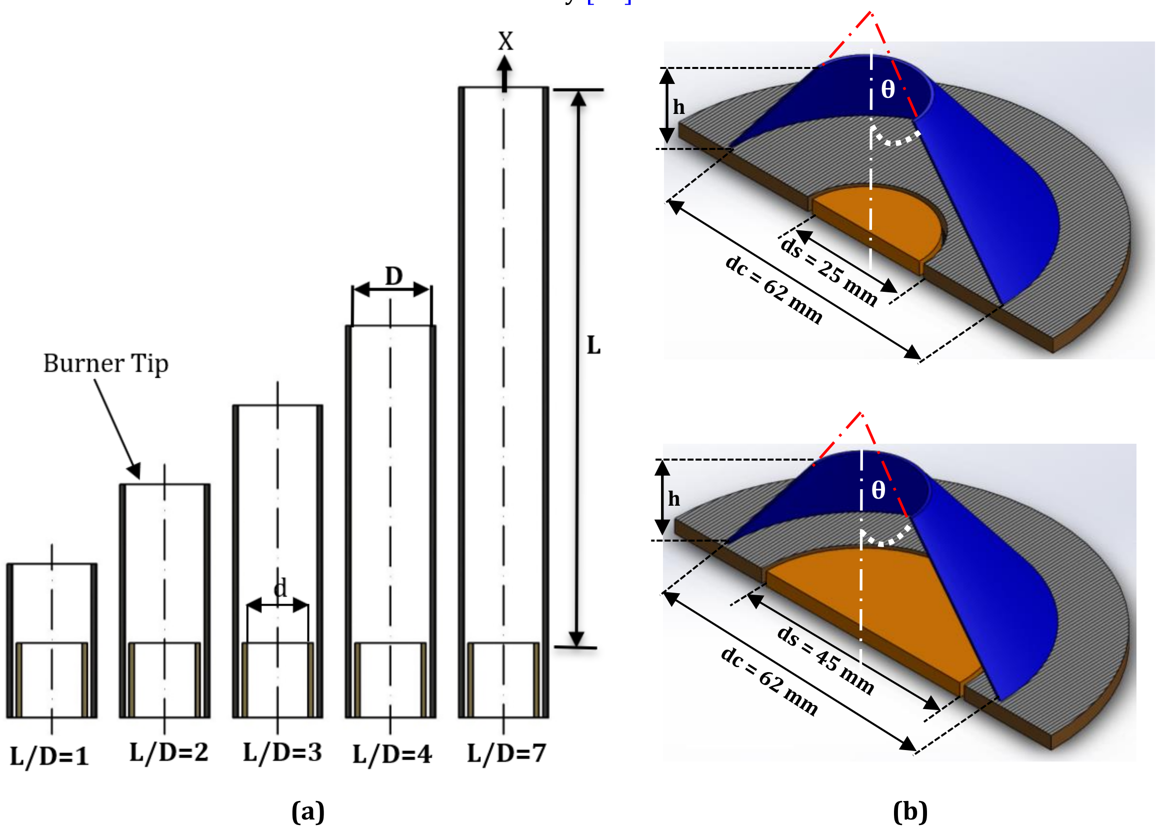

Figure.2. (a) Sets of 5 different levels of partial premixing (L/D), and (b) Different slit diameters (ds = 25 mm and 45 mm) used for the turbulence generator disks

2.3. LIBS set-up

The schematic diagram of the experimental apparatus used for the LIBS-technique is presented in Figure 3. The plasma was generated by using a pulsed Nd: YAG laser with a frequency of 10 Hz. This laser beam was characterised as the first harmonic wavelength of 1064 nm, pulse width of 6 ns and a beam diameter of 10 mm. Single shot operations of the laser were used for the current investigation, with a constant laser energy of 100 mJ, whilst the focusing process of the laser beam was carried out using a 50 mm focal length plano-convex lens to create the plasma. This plasma constitutes of excited atoms in the ionized gas, and during the subsequent decay of the excited electrons, a rainbow of light of different wavelengths is released, resulting in characteristic spectral emissions. In order to optimize the spectral emission data collections, a pair of 100 mm focal-length plano-convex lenses were placed at an angle of 26° to the laser beam [9], and then the spectral emissions were directed towards a fused-silica optical fiber with an aperture of 200 μm. Consequently, the spatial resolution of the system based on this aperture diameter was small enough for turbulent flame measurements and it was approximately 1 mm, estimated from the size of the plasma. Consequently, the optical fiber captured the emitted light and it carried it to an Echelle spectrometer (PI-Echelle, Princeton Instruments: IMAX-512, USA) attached to a gated Intensified Charge-Coupled Device (ICCD) covering a wavelength range of 190–1100 nm, to resolve and image the signal spectrally. The data acquisition system was utilized to precisely control both the gate delay time and the gate width of the spectroscopic data acquisition system. In order to achieve high measurement accuracy, the laser induced plasma generated should reach the Local Thermodynamic Equilibrium (LTE) state, and for the current investigation, the LTE was established at roughly 1 μs following the plasma initiation.

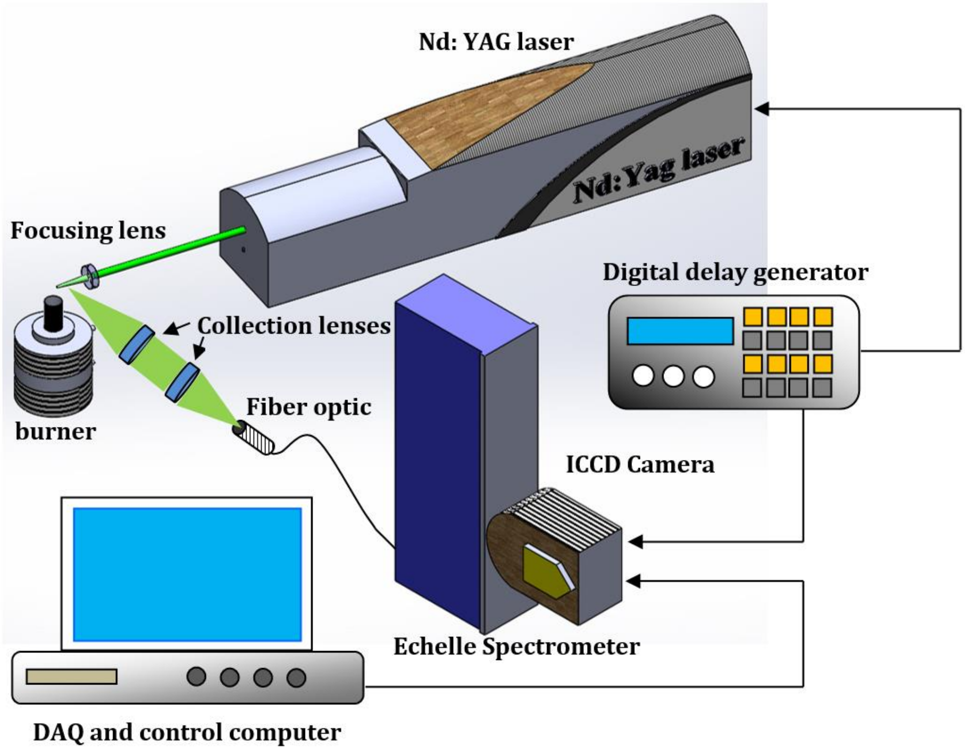

Figure.3. Schematic diagram of the LIBS setup

A Stanford research model DG535 4-channel delay pulse generator was employed to precisely control the Shutter timing of the ICCD camera and the laser-trigger signals. A precise control of the timing parameter and delay time was carried out by combining the fast oscilloscope (500MHz) with the fast photodiode (rise time = 1 ns). The spectral emission lines were analysed and identified using commercial software (GRAMS/AIv.8.0, Thermo-electron. Co.). The raw emission signals collected by the LIBS system were corrected by subtracting them from the emission background by using the LIBS software (Winspexs 21). This correction was applied to eliminate the inherently dark signal associated with the spectrometer detector, which itself is associated with the output LIBS signal. Both the delay time and the gate width were varied until the optimized intensity of the spectral emission line was obtained. In order to achieve that optimized signal, the ICCD gate width was set at 10,000 ns, whilst the spectral emission line intensities were collected at a delay time of 600 ns after the laser irradiation. For the present work, one case was selected for equivalence ratio measurements using the LIBS technique. The NG/air mixture employed for this case study was characterized by an equivalence ratio of φ = 0.8, mass flow rate of 2.91 kg/h and jet velocity of V_j = 1.6 m/s. A long distance pipe, with an approximate length of 200 times the pipe diameter was selected for the fuel-air mixing process, to create a perfectly homogeneous mixture valid for precise calibration with the LIBS technique. Consequently, the equivalence ratio measurements were carried out using the LIBS technique after the calibration process was completed.

3. Results and discussion

3.1. Stability limit characteristics

3.1.1 Stability limit characteristics for each fuel and each disk

The degree of mixture stratification at the exit of the outer tube of the current burner is affected by changing the mixing length to diameter ratio (L/D) and by varying the turbulence generator disk slit diameter. Consequently, these equivalence ratio fluctuations will influence the stability, dynamics and the structure of the flame [34]. Therefore, the flame stability behaviour can be characterized, with particular respect to the blowout characteristics to delineate the extinction regions between different Reynolds numbers and either the degree of partial premixing (L/D) or the equivalence ratio, φ. The blowout limit is identified by the bulk jet velocity, V_j at which a complete flame extinction is occurs. This extinction is carried out by increasing the air flow rate while keeping the fuel flow rate fixed, whereas, the blowout limits are obtained only from visual inspection of the flames [35].

In the present work, the assessment of the burner stability was implemented at lean conditions of $\varphi = 0.8$ for five sets of partial premixing ratios (L/D = 1, 2, 3, 4 and 7) as shown in Figure 4 (a). The investigation of the stability map was accomplished for two types of fuels, NG and LPG, using two turbulence generator disks with slit diameters of ds = 25 and 45 mm. At L/D =1, the flame was considered nearly non-premixed, while at L/D =7, the flame was considered almost fully premixed. Furthermore, qualitative measurements of flame characteristics such as flame shape, height and colour associated with each case have been observed as shown in Figure 4 (b). Five rows of images, which represent a comparison between LPG, and NG, for each disk slit diameter, at different degrees of partial premixing, are presented. It was noticed from Figure 4 (a), that changing the degree of partial premixing or changing the turbulent generator disk slit diameter has a significant effect on the flame stability for both fuels. At L/D =1, the NG/air mixture for both the disk slit diameters exhibited the maximum flame stability, whilst the LPG/air mixture with ds = 45 mm demonstrated the minimum flame stability. These results are further explained with the flame images, where NG demonstrated a stable flame with a blue colour, whilst LPG showed a significant small blue region near the flame base followed by a bright yellow flame with high luminosity. The LPG flames look more like diffusion flames, and consequently, the longer flame height associated with LPG flames can be linked to the flame elongating, to obtain the oxygen available in the ambient air. The blue flame near the base is due to the enhanced local partial premixing. The lower stability of LPG/air mixture in comparison to the NG/air mixture could be attributed to the different properties of the fuels, in particular the Lewis number. As it is well known, both the local stretch rate and the physicochemical parameters including the Lewis number and the laminar burning speed have a significant influence on the turbulent burning speed [36]. Clarke [37] calculated the Lewis number against the equivalence ratio for a range of different fuel-air mixtures that are in common use. For lean mixture conditions, the Lewis number for NG (Le = 0.94 @ $\varphi = 0.8$) was lower compared to that of propane (Le = 1.75 @ $\varphi = 0.8$) and butane (Le = 1.8 @ $\varphi = 0.8$) fuels; the main parts of LPG fuel. Consequently, due to the proximity of the NG Lewis number to unity, the turbulent burning velocity of NG flames was enhanced, and hence, the stability of the turbulent NG flames in comparison to LPG flames was improved [38-40]. Furthermore, the laminar flame speed of the NG/air mixture at lean equivalence ratio of $\varphi = 0.8$ was slightly higher compared to that of the LPG/air mixture [41, 42]. Therefore, the NG flames were more stable compared to the LPG flames.

In addition, for L/D =1, both the fuels with disk, ds = 45 mm yielded the minimum flame stability compared to the other L/D ratios. This behaviour could be linked to the lower mixing time (τ_{mix}) generated from the higher turbulence level associated with the large slit diameter [43]. The numerical analysis of the current burner using three-dimensional computational fluid dynamics (CFD) modelling quantified the higher axial and radial turbulent intensities accompanied with disk, ds = 45 mm, compared to that of disk, ds = 25 mm [42]. Consequently, improper air/fuel mixing will be generated during this shorter mixing length, L, due to the insufficient time available for the mixing process. Subsequently, an incomplete partial premixed flame will be produced at the burner tube exit [44], in comparison to the other L/D ratios, which contained longer mixing lengths. Furthermore, when the mixing time of the fuel and air during the burner mixing length becomes shorter than the chemical reaction time ($\tau_c > \tau_{mix}$), the combustion can no longer be sustained, and this will reduce the flame stability. In addition, for the high levels of turbulence intensities, the flame will be quenched quickly, due to the higher mixing rate (scalar dissipation rate), characterized by the small length scale of the turbulence, in comparison to the smaller thickness (δ) of the laminar flame reaction-diffusion zone [45, 46].

As the degree of partial premixing was increased to L/D = 2 and 3, the flame stability was increased for all of the cases, except the case of the NG/air mixture with ds = 25 mm, where the flame stability was gradually reduced. For both partially premixing ratios of L/D = 2 and 3, the LPG/air mixture with ds = 45 mm consistently had the minimum flame stability. The maximum flame stability was achieved at L/D = 3 for LPG with disk, ds = 25 mm and NG with disk, ds = 45 mm. This could be attributed to the multi-reaction zones structure associated with a non-homogeneous mixture, which include lean, rich and diffusion [47].

Once these zones interacted, the likelihood of the triple flame structure formation increased, resulting in higher flame stability [48, 49]. Regarding the flame images, all of the cases exhibited stable flames with a blue colour, except LPG, ds = 45 mm, which yielded a lower stability with a small blue region near the flame base followed by bright yellow flame with high luminosity.

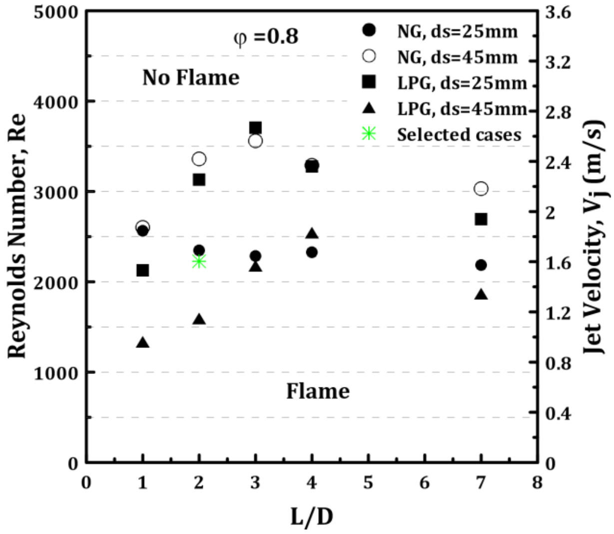

(a)

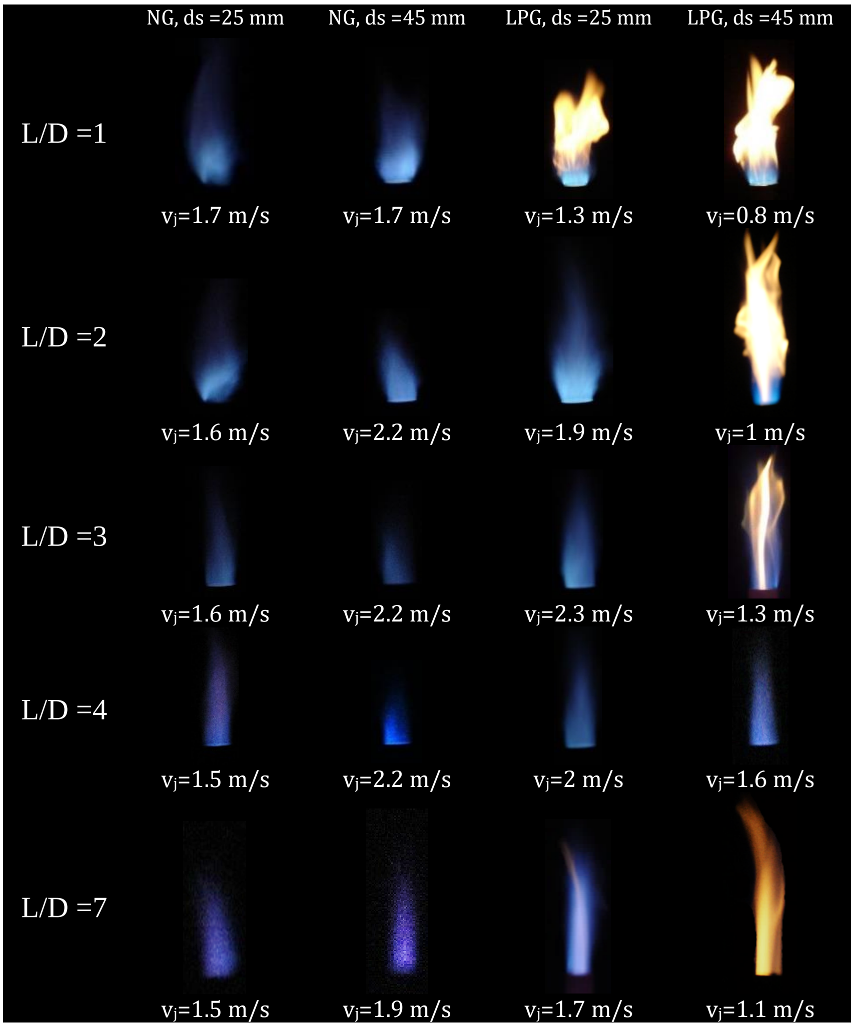

(b)

Figure.4. Impact of changing the disk slit diameter, fuel type and the level of partial premixed on (a) stability curves and (b) flame appearance of partially premixed flames.

However, with further increase of the degree of partial premixing to L/D = 4, the flame stability started to decrease for the NG/air mixture with ds = 45 mm, and the LPG/air mixture with ds = 25 mm, whilst the flame stability started to increase for the NG/air mixture with ds = 25 mm, and the LPG/air mixture with ds = 45 mm. The minimum flame stability for the NG/air mixture was produced with ds = 25 mm. In the most well-mixed case of partial premixed degree L/D = 7, it was noticed that the flame stability was reduced for all of the cases.

Figure 4 (a) also demonstrated the evolution of the jet velocity (where the blowout occurred) as a function of the level of the partially premixed L/D. For disk, ds = 25 mm, the maximum jet velocity of V_j =1.8 m/s was observed for NG at L/D = 1, whilst for LPG, the maximum jet velocity of $V_j \approx 2.6$ m/s was observed at L/D = 3. For disk, ds = 45 mm, the maximum jet velocity of $V_j = 2.6$ m/s was observed for NG at L/D = 3 whilst for LPG, the maximum jet velocity of $V_j \approx 1.8$ m/s was observed at L/D = 4. This enhancement in flame stability for these non-homogenous mixtures is linked to the higher probability of finding near-stoichiometric mixtures of fuel and air burning in contact with the hot burnt gases from the burner. This results in additional heat release at the base of the turbulent jet flame and helps to stabilize it.

The flame stability at a constant level of partially premixed of L/D = 2 was further examined under different Reynolds numbers and equivalence ratios, as presented in Figure 5 (a). Furthermore, qualitative measurements of flame characteristics, such as flame shape, height and colour, associated with each case, have been observed, as shown in Figure 5 (b). Four rows of images, which represent a comparison between LPG and NG, for two disk slit diameters of ds = 25 mm and ds = 45 mm, at different equivalence ratios, are displayed. The blowout limit was determined by maintaining a constant mass flow rate of the fuel stream whilst increasing the mass flow rate of the air stream until the flame extinction happened. Four extinction curves were established for each disk slit diameter and each fuel type. For the NG/air mixtures, changing the turbulence generator disk slit diameter had a small effect on the flame stability, especially at very lean conditions, where their behaviours were closely matched. On contrast, the flame stability of the LPG/air mixture was more susceptible to the change of the turbulence generator disk slit diameter. For lean mixture conditions of $\varphi < 0.8$, the LPG/air mixture with ds = 25 mm yielded the maximum flame stability followed by the NG/air mixtures with ds = 45 mm and 25 mm, respectively. The flame stability completely deteriorated for the LPG/air mixture with ds = 45mm, over the whole equivalence ratio range. The higher stability of LPG at lean conditions could be contributed to its higher calorific value (energy content) than natural gas, with 93.2 MJ/m^3 vs 38.7 MJ/m^3 [50], and thus, its higher heat release rate. The primary effect of an increase in the heat released by the flame is to increase the flame speed, and consequently, a small amount of LPG will produce a higher energy flame as compared to an equivalent amount of NG [51, 52]. A slightly higher flame stability was observed for the NG/air mixture, for the disk slit diameter of ds = 25 mm, as compared to disk slit diameter, ds = 45 mm, for lean conditions ($\varphi < 0.6$). This was due to the high susceptibility of the combustion systems operating at lean conditions to the high turbulence accompanied with ds = 45 mm, which promoted lower flame stability induced by local flame extinction [53]. Consequently, this resulted in lower thermal diffusivity compared to the mass diffusivity and hence the rate of heat transfer could not keep pace with the rate of mass transfer, resulting in the flame becoming quenched.

For equivalence ratios of $\varphi \geq 0.8$, the NG/air mixture with ds = 45 mm demonstrated the maximum flame stability followed by the LPG/air mixture with ds = 25 mm, and the NG/air mixture with ds = 25 mm. A significant difference in the flame stability for the NG/air mixture with ds = 45 mm was noticed at the equivalence ratios of $\varphi = 0.8$ and 0.9, as compared to that observed with ds = 25 mm. The high turbulence level associated with the large disk ds = 45 mm, resulted in an increase in the entrainment of the hot product gas and flame radicals towards incoming reactants, elevating the chemical reaction rate and hence the stabilization of the flame [54, 55]. LPG with ds = 45 mm, consistently had the minimum burner stability.

Regarding the flame appearance, it was noticed for the NG/air mixtures, that the flame is more stable for both the disks, with a blue colour. In contrast, LPG with ds = 45 mm, yielded a completely diffusive flame with a bright yellow colour, without blue coloured flame near its base at very lean mixtures. As the equivalence ratio increased to rich conditions, the flame colour became blue. Likewise, the flame images reflected the higher stability of the flame associated with LPG, ds = 25 mm, for lean conditions, with a longer blue coloured flame near to the base of the flame with a small yellow coloured portion at the top of the flame. Additionally, for stoichiometric and rich conditions, the flame became more stable, with a blue colour.

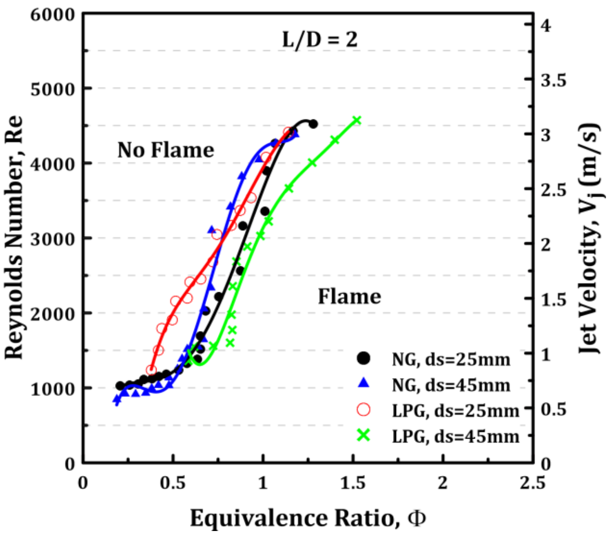

(a)

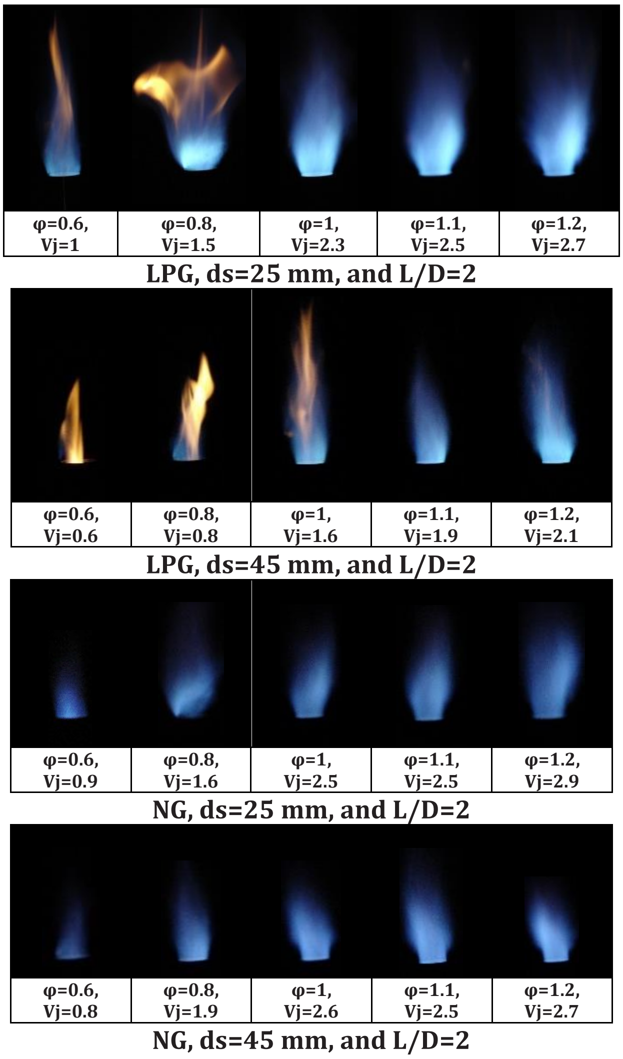

(b)

Figure.5. Impact of changing the disk slit diameter and fuel type on (a) stability curves (b) flame appearance of partially premixed flames at constant level of partial premixing, at L/D = 2.

3.2. LIBS spectra lines and calibration Lines

3.2.1. LIBS spectra

For turbulence disk slit diameter of ds = 25mm, the break down LIBS spectrum, in the region between 240 and 900 nm was measured for the lean NG/air mixture of $\varphi = 0.8$ and jet velocity of $V_j = 1.6$ m/s, as shown in Figure 6. The incident laser energy was maintained constant at 100 mJ for all measurements, and the presented spectrum corresponded to an average of 50 laser shots. A broad band Echelle spectrometer was employed to collect the emission signal and the most common spectral atomic lines highlighted in the spectrum were C (I)-247.8 nm, Hα (I) - 656.4 nm, N (I)-747.2 nm and O (I)- 777.5 nm. Moreover, the N(I) atomic line consisted of three peaks at 742.5, 744.5, and 746.8 nm.

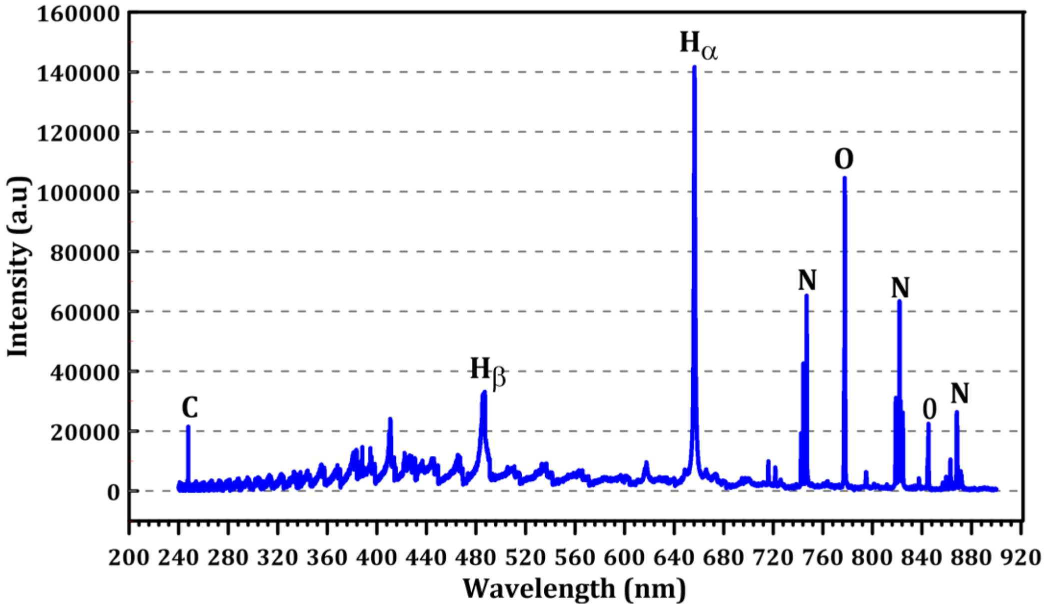

Figure.6. NG/air mixture typical break down LIBS spectrum in the region between 240 and 900 nm at an equivalence ratio of $\varphi = 0.8$.

The quantitative analysis of the local equivalence ratio measurements by the LIBS technique could be fulfilled by establishing a linear relationship between the value of the emission lines intensities and the equivalence ratio of a well premixed mixture. To ensure confidence regarding the high mixture homogeneity, a long-distance pipe with an approximate length of 200 times the pipe diameter was selected for the fuel-air mixing process, to create a perfectly homogeneous mixture. For the calibration purpose, a wide range of equivalence ratios, including eight sets of φ = 0, 0.2, 0.4, 0.6, 0.6, 0.8, 1 and 1.4 were selected to evaluate the emission spectral line intensities of O (I), Hα (I), C (I), and N (I), for each set. The statistical analysis of the emission spectrum was conducted by using the GRAMS/AI V.8.0 Spectroscopy software package. The predominant atomic lines of C (I)-247.8 nm, H_α (I) - 656.4 nm, N (I)-747.2 nm and O (I) - 777.5 nm for each equivalence ratio are presented in Figure 7. Based on the 50 single shot measurements carried out at each set, the calculated standard deviation of the predominant spectral line emission intensities was altered between 5-12%. The spectrum lines were captured with a 0.02 nm spectral resolution by using an ICCD camera attached to an Echelle spectrometer. Due to the air compositions which include 78.09% nitrogen, 20.95% oxygen, 0.93% argon, and 0.04% carbon dioxide, the carbon emission spectral line C (I) was noticed at an equivalence ratio of $\varphi = 0$. The increase of the equivalence ratio was associated with an increase in the intensity of C and H and a decrease in the intensity of O and N.

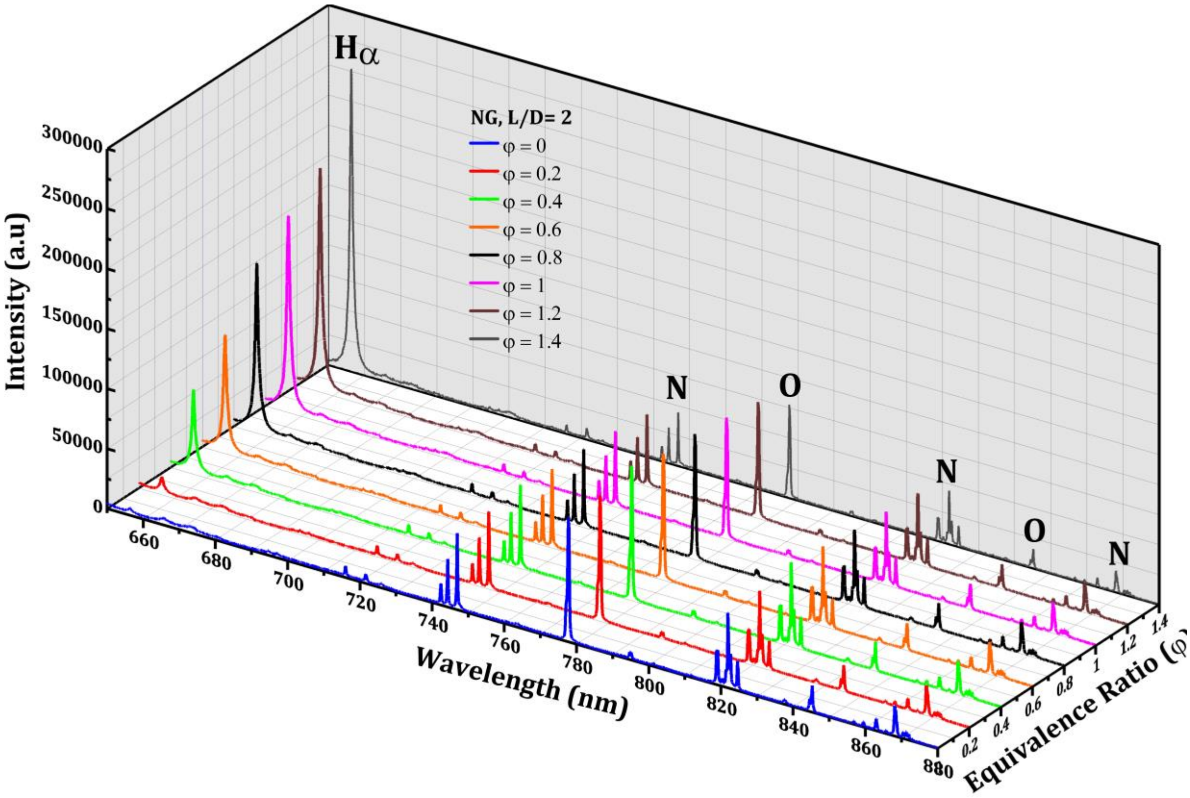

(a)

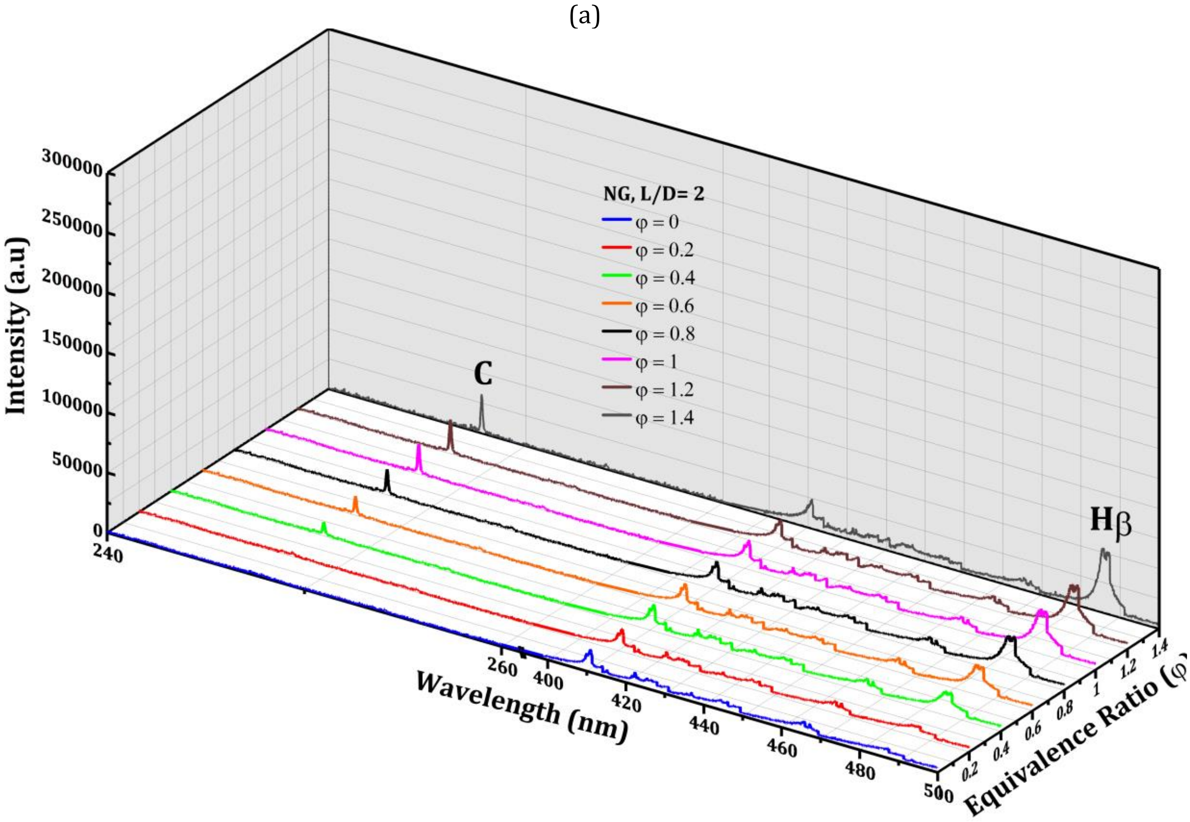

(b)

Figure.7. The LIBS spectra of C (I), H (I), N (I) and O (I) elements for a series of different equivalence ratios at φ = 0, 0.2, 0.4, 0.6, 0.8, 1, 1.2 and 1.4 for the NG/air mixture in the region between (a) 650-880 nm, and (b) 240-500 nm.

3.2.2. Calibration lines

From the spectrum analysis implemented in the aforementioned section, the elemental mass fractions Y_C, Y_H, Y_N and Y_O, were calculated and presented against the signal intensity as a linear relationship in Figure 8. Due to the high precision of using the integral method of the area under each spectral line [25, 56], the mass fraction of each emission line was defined by the ratio between the integration area under the peak of this line and the total integration area under the peaks of all of the elemental spectral lines. The normalized signal intensity was obtained by dividing the elemental signal intensity by the maximum intensity of each element. The high linearity between the LIBS signal intensity and the elemental mass fraction shows the high fidelity of the LIBS system for use as a measuring tool for equivalence ratio quantitative measurements. The deviation of carbon and hydrogen elements from linearity at lower concentrations could be contributed to the laser shot-to-shot fluctuation.

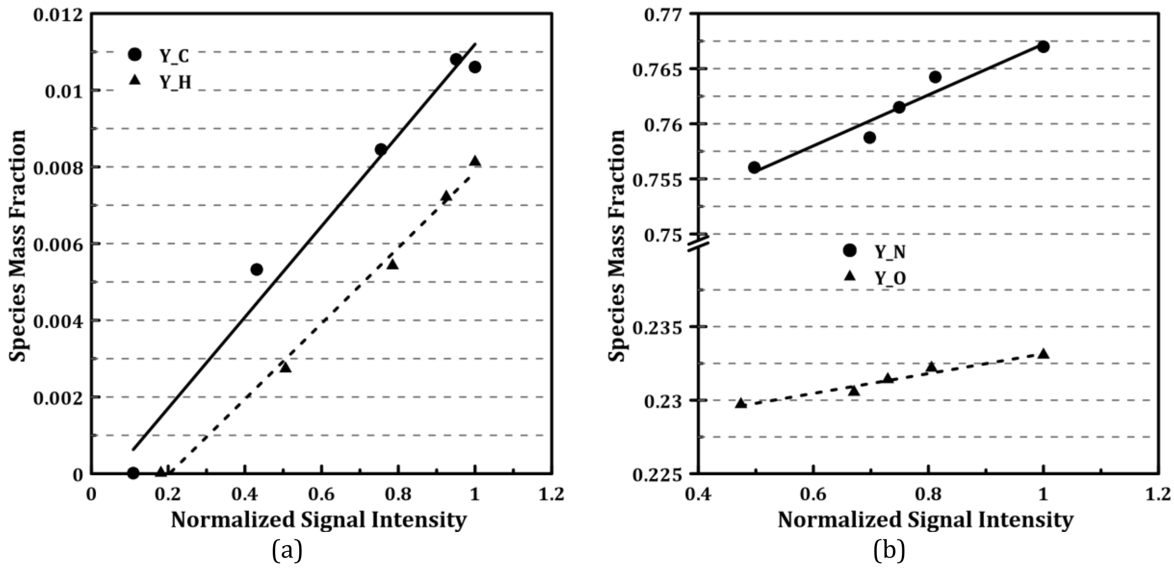

Figure.8. The elemental mass fractions (a) Y_C and Y_H, and (b) Y_N and Y_O, against the normalized signal intensity.

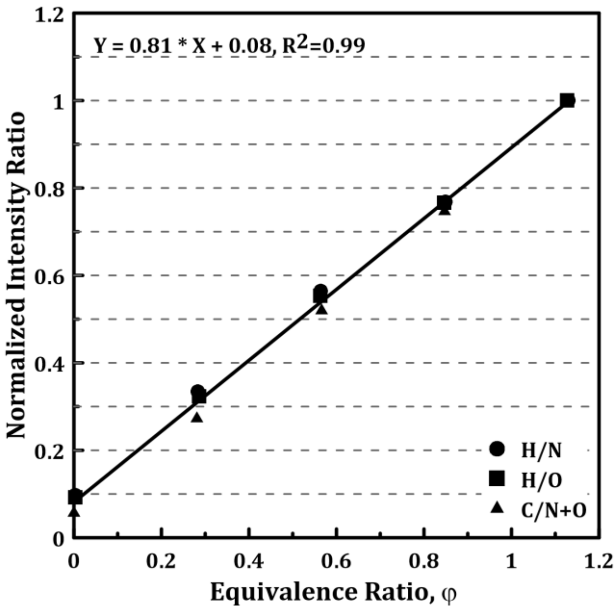

Figure.9. Correlation between the elemental intensity ratio of (a) H/N, (b) H/O and (c) C/N+O, and the equivalence ratio for the premixed NG/air mixture.

The C/(N+O), H/O and H/N intensity ratios were reported as a function of the equivalence ratio for the NG/air mixtures, as shown in Figure 9. The value of each intensity ratio was normalized to the maximum intensity associated with this ratio. Moreover, the three ratios corresponded linearly to the equivalence ratio of the premixed NG/air mixture. This calibration line will be essential for local equivalence ratio measurements. The calibration procedure was accomplished under real temperature and pressure conditions, which is directly related to the behaviour of the flames.

Two methods were utilized to evaluate the mixture fraction (ξ); in the first method, ξ was calculated by using the intensity ratios of C/(N+O), H/N and H/O, whilst the second method identified ξ based on the obtained elemental mass fraction values, which are presented in Figure 8, and substituted it into Eq. (1). Subsequently, a relationship between the two methods is presented in Figure 10. Over the entire range of the mixture fraction measurements, the data showed good agreement, especially with the values determined from the ratio C/(N+O). The intensity ratios of $H_{656.3}/O_{777.4}$ and $H_{656.3}/N_{746.5}$ yielded good agreement with the ξ calculated from Eq. (2), at mixture fractions ξ = 0.03-0.05 and for ξ = 0.07-0.09. Consequently, both methods could be employed for mixture fraction quantitative measurements.

$$\xi = 1 - \sum y_{oi} \qquad \text{Eq (1)}$$

where y_{0i} are the oxidant elements' mass fractions. Thus, ξ for the fuel stream will be 1, and for the oxidizer stream, it will be 0.

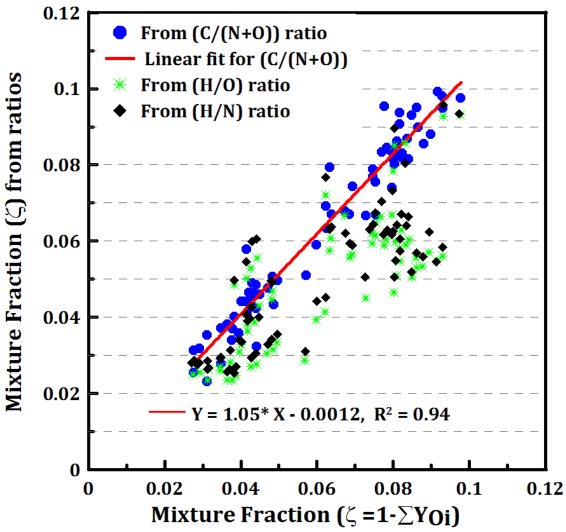

Figure.10. Comparison of the mixture fraction calculation for a partially premixed flame at equivalence ratios of 0.8 and jet velocity of 1.6 m/s, using the three ratios of (C/(N+O)), (H/O) and (H/N), represented by the y-axis, and that calculated from Eq. (2) based on the elemental mass fractions represented by the x-axis.

3.3. Mass Fraction Measurements

The flame appearance and the location of the measurement axial positions (red dots) of the lean partially premixed flame at the equivalence ratio, φ= 0.8, with two disk slit diameters, for the NG/air mixture, is shown in Figure 11.

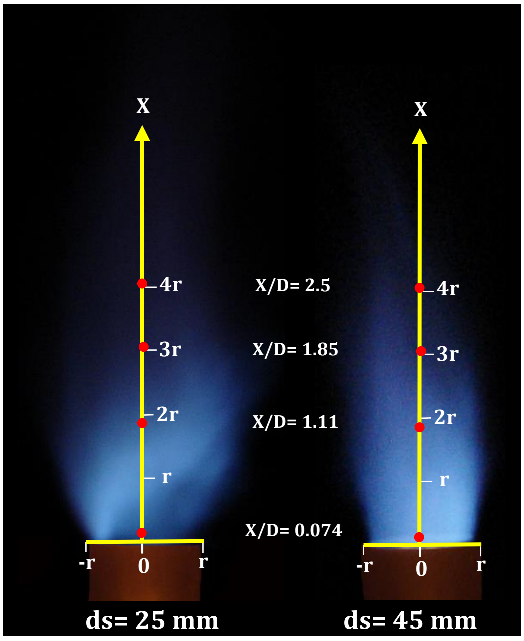

Figure.11. The flame appearance and the location of the measurement axial positions (red dots) of the lean partially premixed flame at the equivalence ratio, φ= 0.8 and V_j= 1.6 m/s, with two disk slit diameters, for the NG/air mixture.

Figure 12 shows the mass fraction radial distribution of different elements including O, N, H and C with the two disk slit diameters of ds = 25 mm and ds = 45 mm, at further distances from the burner rim. Around the burner axis, a perfectly symmetrical distribution of the mass fraction occurred. A perfectly flat shaped distribution occurred with the large slit diameter of ds = 45 mm, whilst a triangular shaped distribution occurred with a lower slit diameter of ds = 25 mm. In comparison to the lower disk slit diameter of ds = 25 mm, the larger disk slit diameter of ds = 45 mm had a lower mass fraction distribution for elements H and C, and a higher oxidant elemental mass fraction of N and O over the radial region of $-0.5 \leq r/R \leq 0.5$. For disk, ds = 45 mm, the reduction in C and H mass fractions at X/D = 0.074 was approximately 8%, and as the distance from the burner rim further increased to X/D = 2.5, the reduction in C and H mass fractions increased up to 30% in comparison to those observed with the disk, ds = 25 mm. This can be understood by referring to the numerical analysis of the current burner, which showed that the large disk, ds = 45 mm, was associated with higher turbulence intensity, and subsequently, the mixing layer during the burner mixing length, L, will be changed [43]. This higher intensity will be associated with a large rate of strain, which reduced the annulus fuel stream, to entrain more into the air stream and the rate of molecular diffusion will be reduced, resulting in higher Y_N & Y_O and lower Y_C, & Y_H [57-59].

The elemental mass fraction of H and C were reduced for both disks, as the distance from the burner rim increased further, due to the increased time available for the surrounding air to penetrate into the partially premixed flame [26]. It was noticed that the elemental mass fraction of H and C were reduced for both the disks as the distance from the burner rim further increased due to the increased time available for the surrounding air to penetrate deeper into the partially premixed flame. Furthermore, at the edge of the burner the values of the elemental mass fraction of O and N were very close to that components of atmospheric air, and moving toward the burner centerline, these values were reduced. This could be linked to the shear layer generated due to the diffusion between the air and fuel.

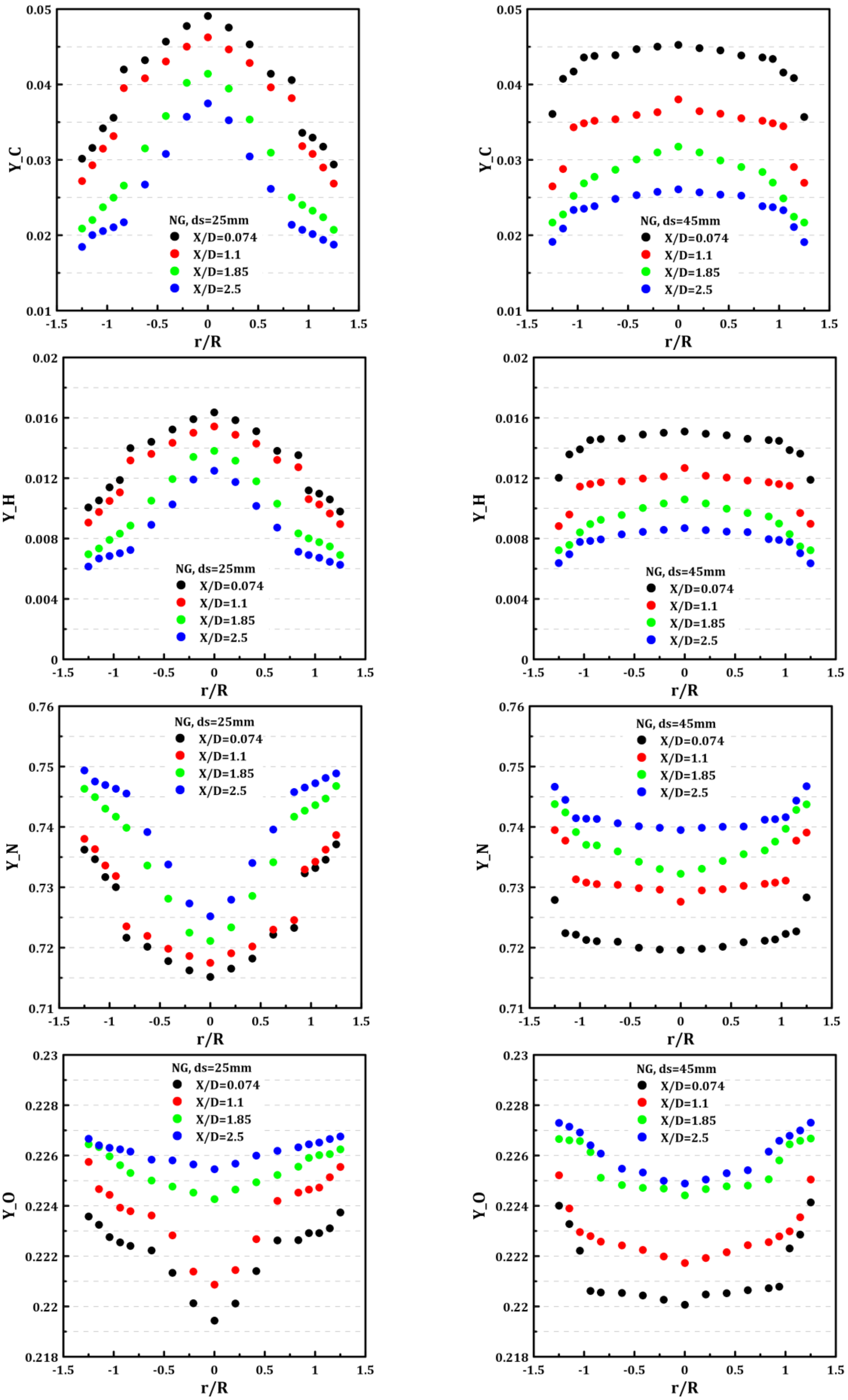

Figure.12. Effect of changing the disk slit diameter on the elemental mass fraction distributions for the lean partially premixed flame of φ = 0.8 at different axial positions for the NG/air mixture.

3.4. Mixture Fraction Measurements

Based on the calibration curves shown in Figure 9, the local equivalence ratio could be identified for each measured point according to any of the three intensity ratios C/(N+O), H/N and H/O. The local equivalence ratio was calculated as an average of 50 laser shots. Then the mixture fraction ξ can be either calculated based on the obtained elemental mass fractions values presented in Figure 8 and substituted in Eq. (2), or by using the local equivalence ratio determined from the linear calibration trend and substituting it into Eq. (3):

$$\xi = \sum y_{Fi} \tag{2}$$

where y_{Fi} are the fuel elements' mass fractions. Furthermore, the mixture fraction, ξ can be employed to evaluate the average equivalence ratio based on Eq. (3):

$$\xi = \frac{\varphi}{\varphi + (\frac{A}{F})_{st}} \tag{3}$$

For the current NG/air flame the stoichiometric air-to-fuel ratio$(A/F)_{st}$ was calculated as 17.167.

The impact of changing the disk slit diameter on the mean radial profile distribution of equivalence ratio or mixture fraction at different axial positions of X/D = 0.074, 1.11, 1.85 and 2.5 are presented in Figure 13. All of the measurements were conducted at lean NG/air mixture conditions of φ = 0.8, V_j = 1.6 m/s and partially premixed degree of L/D = 2, to investigate the structure of the flame. The results demonstrated that the equivalence ratio distributions were significantly influenced by altering the disk slit diameter, due to variation of both the mean flow structure and the level of turbulence intensity associated with each disk [60].

Figure 13 illustrates that around the burner axis, a perfectly symmetrical distribution of the mixture fraction, ξ profile was manifested, and the mixture fraction values peaked at the burner axis and rapidly decreased towards the periphery (air side), especially for lower disk slit diameter, ds = 25 mm. This could be interpreted by referring to the numerical investigation of the turbulent intensity produced from the current burner at L/D = 2 [43]. It was noticed that disk ds = 25 mm had a faster decay rate of the turbulent intensity during the mixing length, L, in comparison to that of ds = 45 mm. Consequently, a higher percentage of the fuel introduced through the annulus will be diffused towards the burner centerline for ds = 25 mm during the mixing length, L. The higher level of intensity associated with the large disk, ds = 45 mm, yielded eddies of sufficient strength and with a large rate of strain, which enhanced the entrainment of the annulus fuel to the air stream. As a result, a homogenous mixture fraction distribution will be produced and this was consistent with the results of Meares and Masri [61], where the fuel was introduced by the same way.

As shown in Figure 13, the smaller turbulence generator disk slit diameter of ds = 25 mm consistently encompassed a wide range of equivalence ratios distributions in comparison to that of ds = 45 mm. At an axial distance of X/D = 0.074, the radial distribution of φ for disk ds = 25 mm was varied from very lean condition of φ = 0.67 to very rich conditions of φ = 1.25, whilst for the disk ds = 45 mm, the radial local equivalence ratio profiles were varied from a slightly lean condition of φ = 0.86 to a slightly rich condition of φ = 1.1. As the axial distance from the burner rim further increased, the radial distribution of φ became narrower and the flames were naturally anchored to the burner lips and they took a conical shape, especially at an axial distance of X/D = 2.5 for ds = 25 mm [62]. Furthermore, the disk slit diameter, ds = 45 mm, had a perfectly flat local equivalence ratio distribution for axial distances of X/D = 0.074 and 1.11, within the burner wall boundary. Also, the created flammable region for disk, ds = 25 mm, was decreased from rich condition around φ = 1.25 on the jet axis to stoichiometric conditions at r/R = 0.5 and then to lean conditions, while moving radially further toward the air side. For the disk, ds = 45 mm, a rich homogeneous mixture of φ=1.1 was radially distributed over the burner wall boundary and then started to decrease into stoichiometric and lean conditions at the periphery (air side).

The high turbulence level associated with the large disk, ds = 45 mm, resulted in an increase in the entrainment of the hot product gas and flame radicals towards incoming reactants, elevating the chemical reaction rate, and hence, it helped to stabilize the flame [63-65]. Furthermore, this kind of mixing between the products and reactants diluted the mixture fraction of disk, ds = 45 mm, as compared to that of disk, ds =25 mm. The reduction in mixture fraction values at distances further from the burner rim can be mainly attributed to the enough time available for the surrounding air to penetrate deeper into the partially premixed flame [26]. Moreover, the mixture fraction flat distribution profiles highlight the ability of the current burner configuration to generate highly stable partially premixed flames. In addition, previous studies [8, 66] showed that the flame speed is directly proportional to the mixture fraction gradient and subsequently the flame front curvature. Consequently, the non-uniformity in the ξ distribution increased the flame front curvature and decreased the rate of heat transfer from the flame front, resulting in a lower preheating of the unburned gas layers, and hence, a lower flame propagation speed will be produced [8].

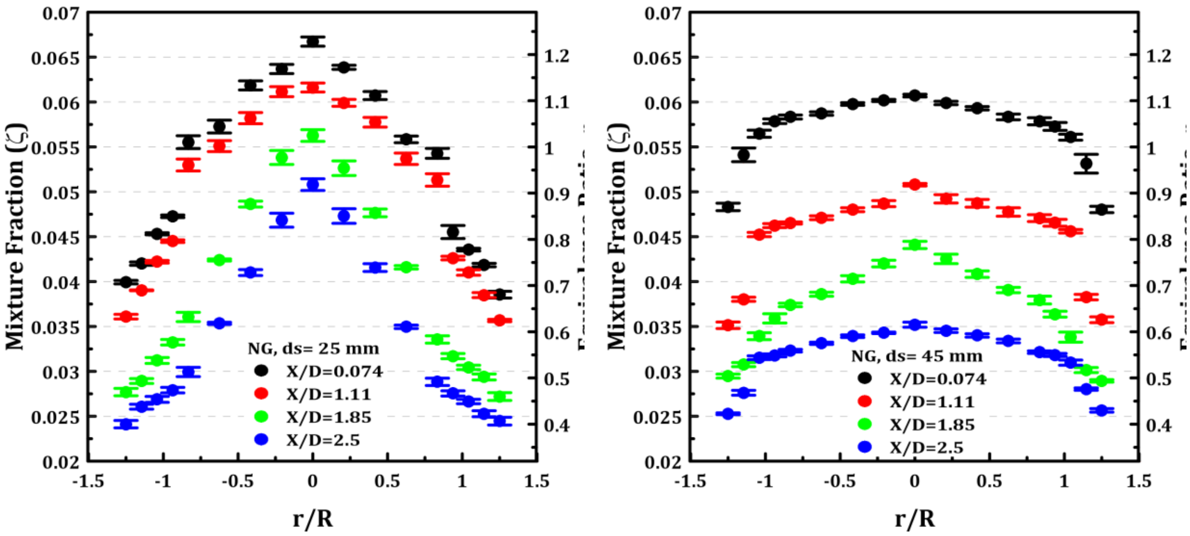

(a) (b)

Figure.13. Impact of changing the disk slit diameter (a) ds = 25 mm and (b) ds = 45 mm, on the mean radial profiles of equivalence ratio or mixture fraction distributions for the NG/air mixture at φ = 0.8, V_j = 1.6 m/s and L/D =2 for certain axial distances.

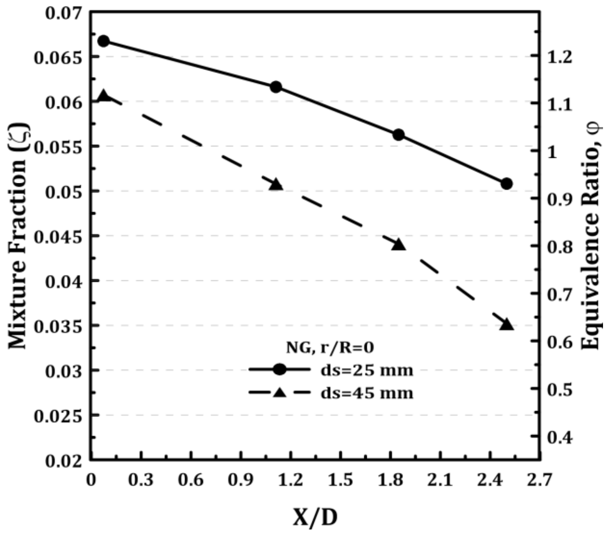

Figure.14. Variation of the equivalence ratio at different axial positions from the burner tip along the burner centerline with different disk slit diameters of ds = 25 mm and ds = 45 mm, for the NG/air mixture at φ = 0.8, V_j =1.6 m/s and L/D =2.

Figure 14 highlighted the reduction of the equivalence ratio with the increase of the axial distances along the burner centerline for different disk slit diameters. Consistently, disk, ds = 25 mm had a higher equivalence ratio at all the axial distances in comparison to disk, ds = 45 mm. This influence was mainly linked to the enhancement of the surrounding air entrainment due to the higher level of turbulence intensity associated with the large disk, ds = 45 mm. As the axial distance above the burner tip increased from 0.074 to 2.5, the equivalence ratio was reduced for both the ds = 25 mm and ds = 45 mm disks by approximately 25% and 43%, respectively. In addition, at an axial distance of X/D = 0.074, the equivalence ratio for disk, ds = 25 mm, was higher than that of disk, ds = 45 mm, with approximately 9.6%. As the axial distance from the burner tip increased to X/D = 2.5, the difference in the equivalence ratio between disk, ds = 25 mm and disk, ds = 45 mm, increased up to approximately 32%.

The fluctuation in mixture fraction were calculated as a ratio between the root mean square of the mixture fraction fluctuations and the average of the mixture fraction values along the burner centerline. Both the mean and fluctuating mixture fraction profiles (ξ and ξ^*, respectively) are presented in Figure 15 for an axial distance of X/D = 0.074. For the lower disk slit diameter, ds = 25 mm, and lean mixture of φ = 0.8, higher fluctuations occurred within the burner wall boundary compared to those observed with disk, ds = 45 mm. In contrast, outside the burner boundary disk, ds = 25 mm yielded lower fluctuations compared to disk, ds= 45 mm. At X/D = 0.074 and $-1 \leq r/R \leq 1$, the peak fluctuation for disk, ds = 25 mm, was approximately 0.028, whilst for disk, ds = 45 mm, it was approximately 0.017. Moreover, across the burner region of $-0.5 \leq r/R \leq 0.5$, the mixture fraction fluctuation associated with the disk, ds = 45 mm, was nearly fixed around 0.008, and lower compared to that of the lower disk, ds = 25 mm, with approximately 0.019. Figure 16 shows the fluctuating mixture fraction profiles ξ^* for the NG/air mixture at φ = 0.8 and L/D = 2, at further axial positions from the burner rim. The mixture fraction fluctuation profiles for disk, ds = 45 mm, were consistently lower than that of ds = 25 mm, for most of the radial distances r/R. The maximum fluctuation was noticed for disk, ds = 25 mm at an axial distance of X/D = 2.5 with ξ^* = 0.05. At an axial distance of X/D = 1.11, the fluctuation trends for disk, ds = 25 mm, was slightly higher than that of the disk, ds = 45 mm. While at axial distance of X/D = 1.85, the fluctuation trends for both disks were close to each other.

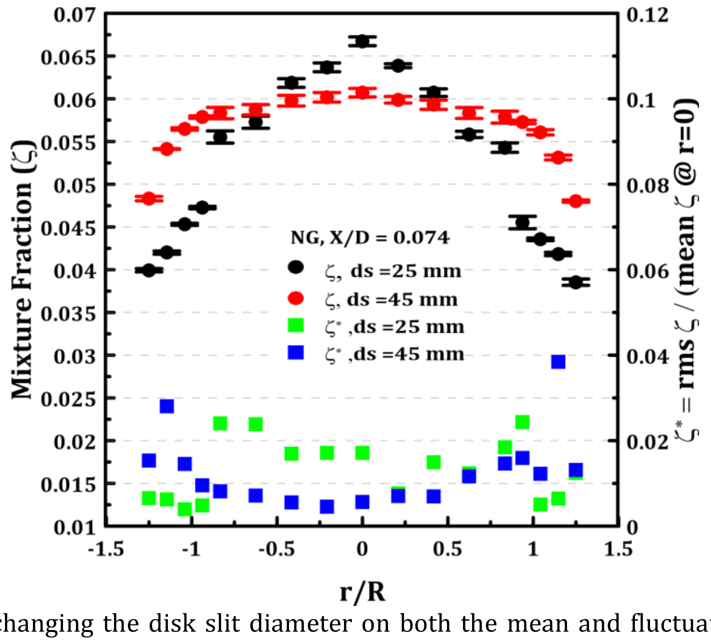

Figure.15. Impact of changing the disk slit diameter on both the mean and fluctuating mixture fraction profiles for the NG/air mixture at φ = 0.8 and L/D =2 for the axial distance of X/D =0.074.

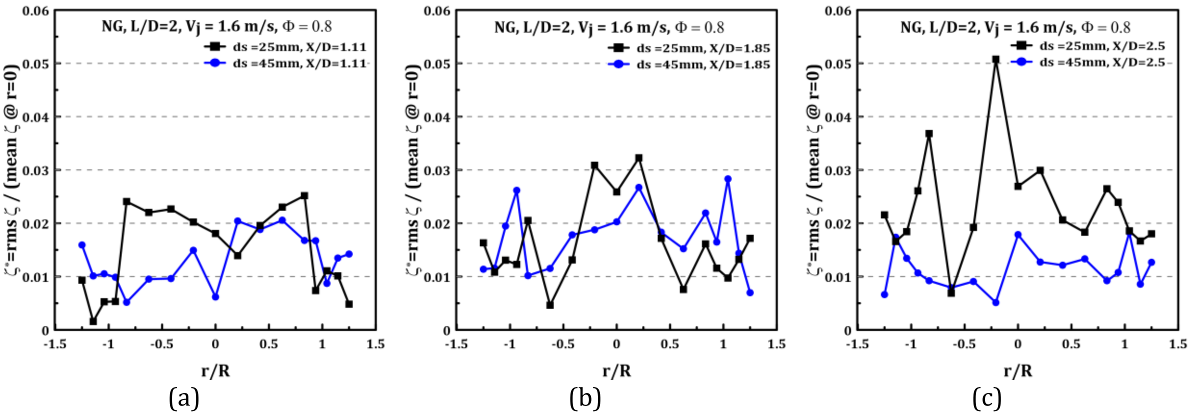

Figure.16. Impact of changing the disk slit diameter on the fluctuation of the mixture fraction profiles for NG/air mixtures at φ = 0.8 and L/D = 2 for axial distances of (a) X/D = 1.1, (a) X/D = 1.85 and (a) X/D = 2.5.

Conclusions

The current study was mainly focused towards the extension of the lean combustion limit by generating higher turbulence levels or by using the partially stratified charge method. Likewise, the burner was designed for improving the stability of lean flames, and consequently, it produces low emissions. In addition, the LIBS technique was employed to characterize and quantify the impact of changing the disk slit diameter on the distribution profiles of equivalence ratio or mixture fraction for NG/air partially premixed flame. The current burner configuration stability was examined for a lean NG/air mixture at φ = 0.8 by changing the disk slit diameters, the fuel used and the degree of partial premixing. The conclusions drawn from this work are as follow:

(1) At the equivalence ratio of φ = 0.8 and for different levels of partially premixing, it was noticed that changing the disk slit diameter has a great impact on the flame stability for both NG and LPG fuels. Increasing the disk slit diameter from ds = 25 mm to ds = 45 mm resulted in a higher flame stability for the NG/air mixture. In contrast, increasing the disk slit diameter for LPG/air mixtures reduced its flame stability.

(2) Changing the level of partial premixing (L/D) lead to an enhancement in the flame stability for both fuels. However, the optimum L/D ratio where the maximum flame stability occurred varied based on which fuel type and disk slit diameter was used. L/D = 1 was the optimum ratio for NG with disk, ds = 25 mm, at which the maximum flame stability was achieved. The maximum flame stability was achieved at L/D = 3 for LPG with disk, ds = 25 mm, and for NG with disk, ds = 45 mm. Finally, for LPG with disk, ds = 45mm, L/D = 4 was the optimum ratio at which the maximum flame stability occurred.

(3) Among all the cases, the NG/air mixture with ds = 45 mm and φ = 0.8 demonstrated the maximum flame stability, whilst the LPG/air mixture with ds = 45 mm and φ = 0.8, yielded the minimum flame stability over different levels of partial premixing.

(4) At a constant level of partially premixing of L/D = 2, it was noticed that for equivalence ratios of φ ≥ 0.8, the NG/air mixture with ds = 45 mm exhibited the maximum flame stability. Whilst for equivalence ratios of φ < 0.8, the LPG/air mixture with ds = 25 mm yielded the maximum flame stability.

(5) The larger disk slit diameter, ds = 45 mm, demonstrated almost zero mixture fraction gradients distributions and lower fluctuation of the mixture fraction distributions within the burner wall boundary in comparison to that of disk, ds = 25 mm, for the NG/air mixture at φ = 0.8 and L/D = 2.

(6) Along the burner centerline disk, ds = 25 mm consistently had a higher equivalence ratio at all of the axial distances in comparison to disk, ds = 45 mm. The equivalence ratio at axial distances of X/D = 0.074 and X/D = 2.5, for disk, ds = 25mm, was higher than that of disk, ds = 45mm, with approximately 9.6% and 32%, respectively. As the axial distance above the burner tip increased from 0.074 to 2.5, the equivalence ratio was reduced for both disks, ds = 25mm, and ds = 45mm, by approximately 25% and 43%, respectively.
(7) The mixture fraction fluctuation profiles associated with disk, ds = 45mm, were consistently lower than that of ds = 25mm, for most of the radial distances r/R. Near the burner tip at X/D = 0.074, the peak

fluctuation for disk, ds = 25mm, was approximately 0.028, whilst for disk, ds = 45 mm, was approximately 0.017. The maximum fluctuation was observed for disk, ds = 25mm, at an axial distance of X/D = 2.5 with $\xi^* = 0.05$.

Acknowledgement

The authors would like to acknowledge the support from Dr Ivan Langella for his advice, support and positive feedback.

References

[1] Temerev AA. Extending the lean limit of methane-air mixtures by oxygen, nitrogen and carbon dioxide injection in the gap of the spark plug's electrodes. 2015.

[2] Bradley D. Combustion and the design of future engine fuels. Proceedings of the Institution of Mechanical Engineers, Part C: Journal of Mechanical Engineering Science 2009;223(12):2751-65.

[3] Tachibana S, Kanai K, Yoshida S, Suzuki K, Sato T. Combined effect of spatial and temporal variations of equivalence ratio on combustion instability in a low-swirl combustor. Proceedings of the Combustion Institute 2015;35(3):3299-308.

[4] Richardson ES, Chen JH. Analysis of turbulent flame propagation in equivalence ratio-stratified flow. Proceedings of the Combustion Institute 2017;36(2):1729-36.

[5] Vena PC, Deschamps B, Guo H, Johnson MR. Effects of stratification on locally lean, near-stoichiometric, and rich iso-octane/air turbulent V-flames. Combustion and Flame 2015;162(11):4231-40.

[6] Xu C, Wang Z, Weng W, Wan K, Whiddon R, Wu A. Effects of the Equivalence Ratio and Reynolds Number on Turbulence and Flame Front Interactions by Direct Numerical Simulation. Energy & Fuels 2016;30(8):6727-37.

[7] Richardson ES, Granet V, Eyssartier A, Chen J. Effects of equivalence ratio variation on lean, stratified methane–air laminar counterflow flames. Combustion Theory and Modelling 2010;14(6):775-92.

[8] Dold J. Flame propagation in a nonuniform mixture: analysis of a slowly varying triple flame. Combustion and Flame 1989;76(1):71-88.

[9] Cremers DA, Knight AK. Laser-Induced Breakdown Spectroscopy. Wiley Online Library; 2006.

[10] Harmon RS, Russo RE, Hark RR. Applications of laser-induced breakdown spectroscopy for geochemical and environmental analysis: A comprehensive review. Spectrochimica Acta Part B: Atomic Spectroscopy 2013;87:11-26.

[11] Pasquini C, Cortez J, Silva L, Gonzaga FB. Laser induced breakdown spectroscopy. Journal of the Brazilian Chemical Society 2007;18(3):463-512.

[12] Gondal MA, Shemis MA, Khalil AA, Nasr MM, Gondal B. Laser produced plasma diagnosis of carcinogenic heavy metals in gallstones. Journal of Analytical Atomic Spectrometry 2016;31(2):506-14.

[13] Romera JPR, Barsanelli PL, Pereira FMV. Expeditious prediction of fiber content in sugar cane: An analytical possibility with LIBS and chemometrics. Fuel 2016;166:473-6.

[14] Noll R. Laser-induced breakdown spectroscopy. Laser-Induced Breakdown Spectroscopy. Springer; 2012, p. 7-15.

[15] Fichet P, Mauchien P, Wagner J-F, Moulin C. Quantitative elemental determination in water and oil by laser induced breakdown spectroscopy. Analytica chimica acta 2001;429(2):269-78.

[16] Charfi B, Harith M. Panoramic laser-induced breakdown spectrometry of water. Spectrochimica Acta Part B: Atomic Spectroscopy 2002;57(7):1141-53.

[17] Sturm V, Peter L, Noll R. Steel analysis with laser-induced breakdown spectrometry in the vacuum ultraviolet. Applied Spectroscopy 2000;54(9):1275-8.

[18] Cabalin L, Laserna J. Experimental determination of laser induced breakdown thresholds of metals under nanosecond Q-switched laser operation. Spectrochimica Acta Part B: Atomic Spectroscopy 1998;53(5):723-30.

[19] Cremers DA, Radziemski LJ. Detection of chlorine and fluorine in air by laser-induced breakdown spectrometry. Analytical Chemistry 1983;55(8):1252-6.

[20] Hanafi M, Omar M, Gamal Y-D. Study of laser-induced breakdown spectroscopy of gases. Radiation Physics and Chemistry 2000;57(1):11-20.

[21] Tripathi MM, Srinivasan KK, Krishnan SR, Yueh F-Y, Singh JP. A comparison of multivariate LIBS and chemiluminescence-based local equivalence ratio measurements in premixed atmospheric methane–air flames. Fuel 2013;106:318-26.

[22] Lee T-W, Hegde N. Laser-induced breakdown spectroscopy for in situ diagnostics of combustion parameters including temperature. Combustion and flame 2005;142(3):314-6.

[23] Kotzagianni M, Yuan R, Mastorakos E, Couris S. Laser-induced breakdown spectroscopy measurements of mean mixture fraction in turbulent methane flames with a novel calibration scheme. Combustion and Flame 2016;167:72-85.

[24] Zimmer L, Yoshida S. Feasibility of laser-induced plasma spectroscopy for measurements of equivalence ratio in high-pressure conditions. Experiments in fluids 2012;52(4):891-904.

[25] Mansour M, Imam H, Elsayed KA, Elbaz AM, Abbass W. Quantitative mixture fraction measurements in combustion system via laser induced breakdown spectroscopy. Optics & Laser Technology 2015;65:43-9.

[26] Phuoc TX, White FP. Laser-induced spark for measurements of the fuel-to-air ratio of a combustible mixture. Fuel 2002;81(13):1761-5.

[27] Michalakou A, Stavropoulos P, Couris S. Laser-induced breakdown spectroscopy in reactive flows of hydrocarbon-air mixtures. Applied Physics Letters 2008;92(8):081501.

[28] Kiefer J, Tröger JW, Li Z, Seeger T, Alden M, Leipertz A. Laser-induced breakdown flame thermometry. Combustion and flame 2012;159(12):3576-82.

[29] McGann B, Carter CD, Ombrello T, Do H. Direct spectrum matching of laser-induced breakdown for concentration and gas density measurements in turbulent reacting flows. Combustion and Flame 2015;162(12):4479-85.

[30] Videto B, Santavicca D. A turbulent flow system for studying turbulent combustion processes. Combustion Science and technology 1991;76(1-3):159-64.

[31] Coppola G, Gomez A. Experimental investigation on a turbulence generation system with high-blockage plates. Experimental Thermal and Fluid Science 2009;33(7):1037-48.

[32] Soulopoulos N, Kerl J, Beyrau F, Hardalupas Y, Taylor A, Vassilicos JC. A turbulent premixed flame on fractal-grid generated turbulence. arXiv preprint arXiv:10042146 2010.

[33] Badawy T, Mansour MS. Assessment of flame kernel propagation in partially premixed turbulent jet under different turbulence levels. Fuel 2017;191:350-62.

[34] Mansour MS, Elbaz AM, Roberts WL, Senosy MS, Zayed MF, Juddoo M, et al. Effect of the mixing fields on the stability and structure of turbulent partially premixed flames in a concentric flow conical nozzle burner. Combustion and Flame 2017;175:180-200.

[35] Guiberti TF, Cutcher H, Roberts WL, Masri AR. Influence of Pilot Flame Parameters on the Stability of Turbulent Jet Flames. Energy & Fuels 2016;31(3):2128-37.

[36] Brequigny P, Halter F, Mounaïm-Rousselle C. Lewis number and Markstein length effects on turbulent expanding flames in a spherical vessel. Experimental Thermal and Fluid Science 2016;73:33-41.

[37] Clarke A. Calculation and consideration of the Lewis number for explosion studies. Process Safety and Environmental Protection 2002;80(3):135-40.

[38] Aspden A, Day M, Bell J. Lewis number effects in distributed flames. Proceedings of the Combustion Institute 2011;33(1):1473-80.

[39] Sánchez–Sanz M, Fernández-Galisteo D, Kurdyumov VN. Effect of the equivalence ratio, Damköhler number, Lewis number and heat release on the stability of laminar premixed flames in microchannels. Combustion and Flame 2014;161(5):1282-93.

[40] Abdel-Gayed R, Bradley D, Hamid M, Lawes M. Lewis number effects on turbulent burning velocity. *Symposium (international) on combustion.* 20. Elsevier; 1985:505-12.

[41] Ibrahim AS, Ahmed SF. Measurements of Laminar Flame Speeds of Alternative Gaseous Fuel Mixtures. Journal of Energy Resources Technology 2015;137(3):032209.

[42] Liao S, Jiang D, Gao J, Huang Z, Cheng Q. Measurements of Markstein numbers and laminar burning velocities for liquefied petroleum gas–air mixtures. Fuel 2004;83(10):1281-8.

[43] Badawy T, Hamza M, Ahmad A, Mansour MS, Abdel-Hafez A-HH, Imam H. New developed burner towards stable lean turbulent partially premixed flames. Fuel 2018;220:942-57.

[44] Moore JD, Risha GA, Kuo KK, D'AGOSTINI MD. Effect of reactant initial temperature on methane/oxygen diffusion flame stability in a furnace. Combustion science and technology 2005;177(11):2069-89.

[45] Gerlach C, Eder A, Jordan M, Ardey N, Mayinger F. Advances in Understanding of Flame Acceleration for the Improving of Combustion Efficiency. Heat Transfer Enhancement of Heat Exchangers. Springer; 1999, p. 395-406.

[46] Lockwood F, Megahed I. Extinction in turbulent reacting flows. Combustion Science and Technology 1978;19(1-2):77-80.
[47] Peters N. Turbulent combustion (Cambridge monographs on mechanics). Cambridge University, Cambridge, UK 2000.
[48] Joedicke A, Peters N, Mansour M. The stabilization mechanism and structure of turbulent hydrocarbon lifted flames. Proceedings of the Combustion Institute 2005;30(1):901-9.
[49] El-Mahallawy F, Abdelhafez A, MANSOUR∗ MS. Mixing and nozzle geometry effects on flame structure and stability. Combustion science and technology 2007;179(1-2):249-63.
[50] Khan N, Manikantachari K, Roy RD, Raghavan V. Experimental Study of Characteristics of LPG-hydrogen Jet Diffusion Flames. Asian Journal of Scientific Research 2013;6(2):227.
[51] Boulanger J, Vervisch L, Reveillon J, Ghosal S. Effects of heat release in laminar diffusion flames lifted on round jets. Combustion and Flame 2003;134(4):355-68.
[52] Ruetsch G, Vervisch L, Liñán A. Effects of heat release on triple flames. Physics of Fluids 1995;7(6):1447-54.
[53] Geikie MK, Ahmed KA. Lagrangian mechanisms of flame extinction for lean turbulent premixed flames. Fuel 2017;194:239-56.
[54] Gupta A, Lewis M, Qi S. Effect of swirl on combustion characteristics in premixed flames. TRANSACTIONS-AMERICAN SOCIETY OF MECHANICAL ENGINEERS JOURNAL OF ENGINEERING FOR GAS TURBINES AND POWER 1998;120:488-94.
[55] Bobba MK. Flame stabilization and mixing characteristics in a stagnation point reverse flow combustor. Georgia Institute of Technology; 2007.
[56] Mansour MS, Imam H, Elsayed KA, Abbass W. Local equivalence ratio measurements in turbulent partially premixed flames using laser-induced breakdown spectroscopy. Spectrochimica Acta Part B: Atomic Spectroscopy 2009;64(10):1079-84.
[57] Drummond JP, Diskin GS, Cutler AD. Fuel-air mixing and combustion in scramjets. 2002.
[58] Pantano C. Direct simulation of non-premixed flame extinction in a methane–air jet with reduced chemistry. Journal of Fluid Mechanics 2004;514:231-70.
[59] Fru G, Thévenin D, Janiga G. Impact of turbulence intensity and equivalence ratio on the burning rate of premixed methane–air flames. Energies 2011;4(6):878-93.
[60] Bedat B, Cheng R. Experimental study of premixed flames in intense isotropic turbulence. Combustion and Flame 1995;100(3):485-94.
[61] Meares S, Masri AR. A modified piloted burner for stabilizing turbulent flames of inhomogeneous mixtures. Combustion and Flame 2014;161(2):484-95.
[62] Kotzagianni M, Kakkava E, Couris S. Laser-induced breakdown spectroscopy (LIBS) for the measurement of spatial structures and fuel distribution in flames. Applied spectroscopy 2016;70(4):627-34.
[63] Kang S, Kim H, Lee J, Kim Y, Chung J-H, Ahn D-H. Stabilization and Combustion Processes of Turbulent Premixed Lifted Methane– Air Flames on Low-Swirl Burners. Energy & Fuels 2008;22(2):925-34.
[64] Cheng T-S, Wu C-Y, Li Y-H, Chao Y-C. Chemiluminescence measurements of local equivalence ratio in a partially premixed flame. Combustion science and technology 2006;178(10-11):1821-41.
[65] Lee T-W, Mitrovic A. Structure of lean turbulent partially-premixed flames stabilized in a co-axial jet flame burner. Combustion science and technology 1997;127(1-6):231-49.
[66] HARTLEY LJ, Dold J. Flame propagation in a nonuniform mixture: analysis of a propagating triple-flame. Combustion science and technology 1991;80(1-3):23-46.